SUPPLEMENTAL MATERIAL

Liu et al., http://www.jem.org/cgi/content/full/jem.20092123/DC1

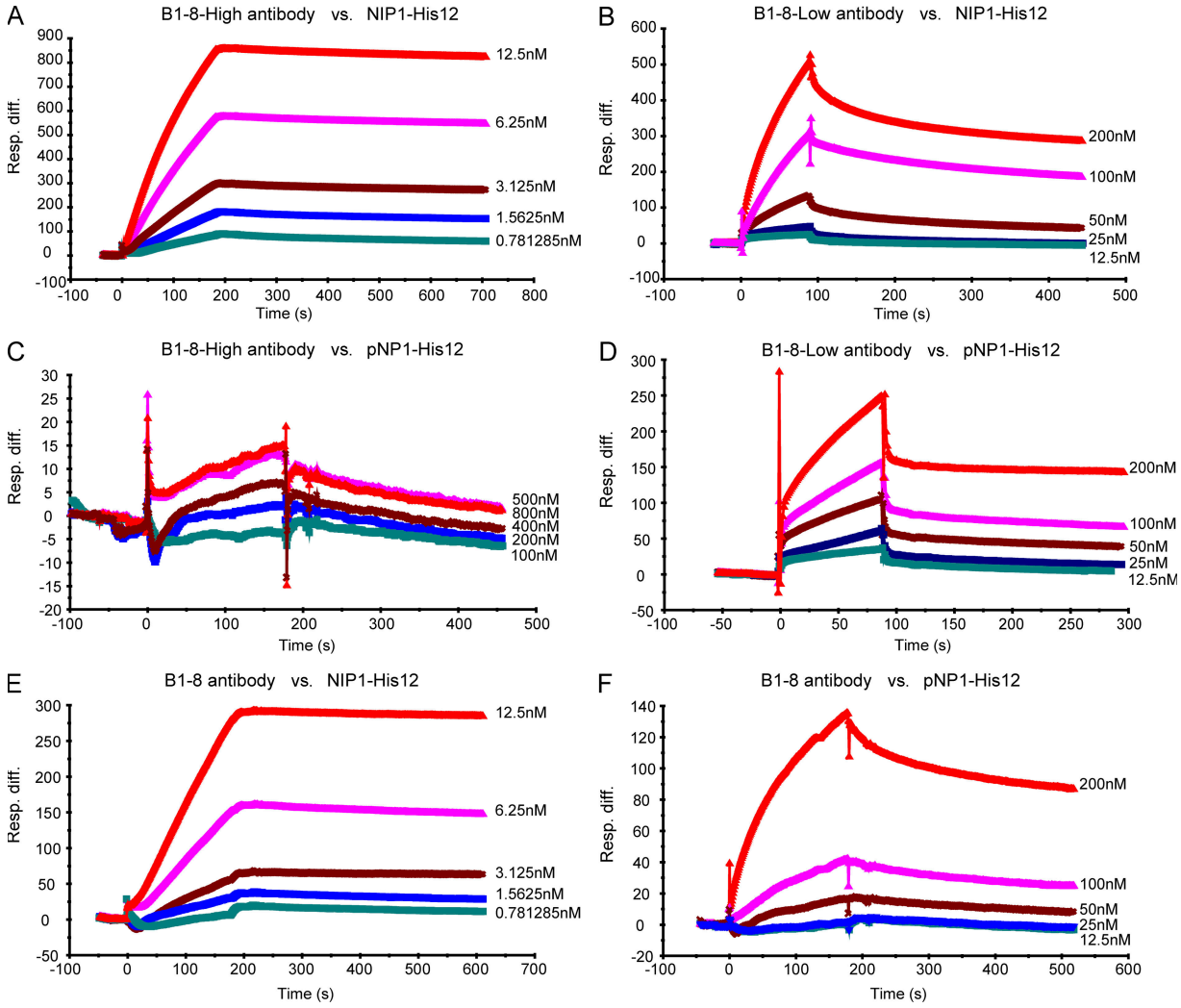

Figure S1. Measuring the real-time association and dissociation kinetics of B1-8 antibodies with NIP1- or pNP1-hapten–conjugated peptide antigen by BIAcore surface plasmon resonance. (A–F) NIP1-His12 (A, B, and E) or pNP1-His12 (C, D, and F) peptide antigen was immobilized on the surface of a CM5 biosensor. Five different concentrations of B1-8-High (A and C), B1-8-Low (B and D), and B1-8 (E and F) antibodies, as indicated in the figure, were flowed through and measured for the real-time association and dissociation kinetics. The kinetic binding curves of each antibody–antigen pair were fitted to the BIAevaluation software to calculate the affinity constant K_A, on-rate $K_{forward}$, and off-rate K_{back} for each antibody–antigen pair as indicated and detailed in Materials and methods. Results are representative of two independent experiments. Resp. diff., the amount of the antibody bound to the immobilized antigen ligand on the chip surface.

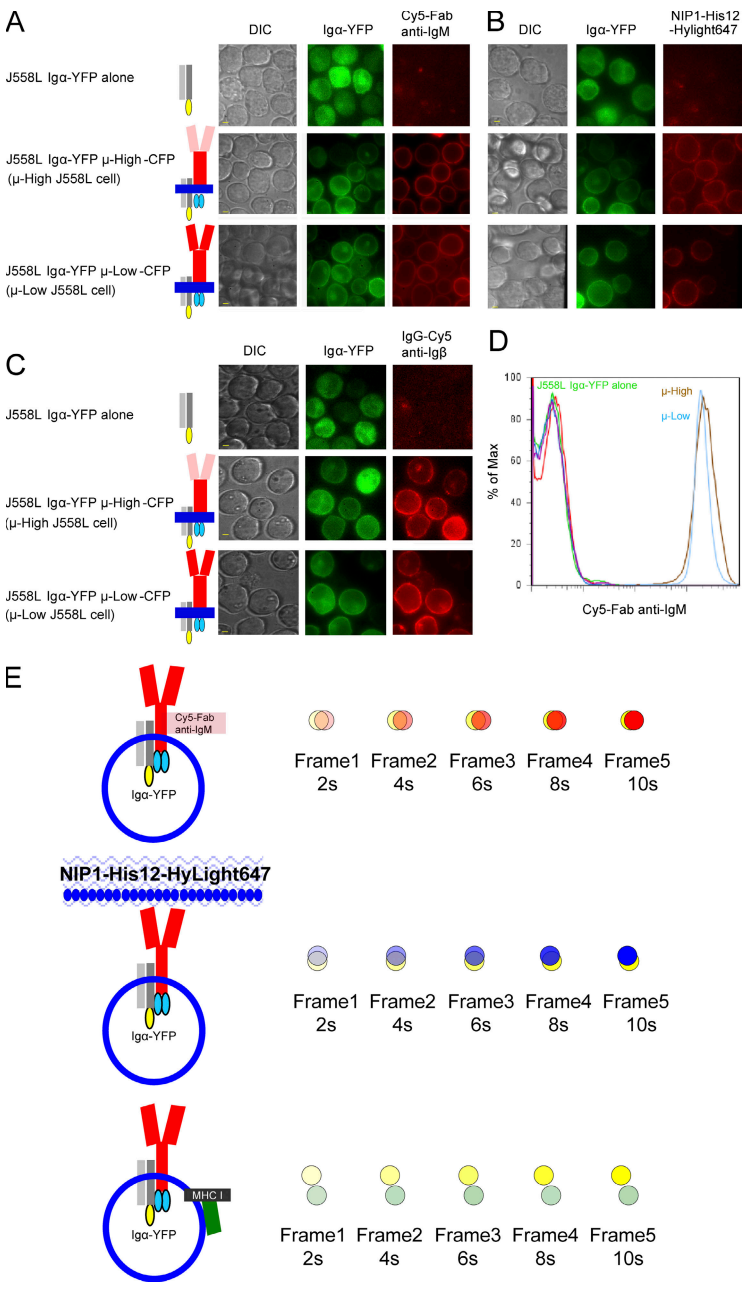

Figure S2. Expression of BCRs on the plasma membrane of μ-High and μ-Low J558L cells and schematic presentation of the experimental design of two-color live-cell imaging in a time-lapse manner in TIRFM. (A–D) J558L cell lines stably expressing Igα-YFP alone, Igα-YFP plus μ-B1-8-High-CFP, or Igα-YFP plus μ-B1-8-Low-CFP were incubated with Cy5-Fab anti-IgM (A and D), IgG-Cy5 anti-Igβ (C), or NIP1-His12-Hylight647 peptide antigen (B). After washing, the expression of surface BCRs was analyzed by microscopy or flow cytometry. Bars, 1.5 μm. Also shown in D are the flow cytometry analyses of the nonstained background control of these three J558L cell lines. Results are representative of two independent experiments. (E) Time-lapse two-color TIRF live-cell imaging is schematically presented in the experiments of imaging BCR microclusters by simultaneously examining Igα-YFP and Alexa Fluor 568–Fab anti-IgM (top), of imaging BCR and antigen microclusters by simultaneously examining Igα-YFP and NIP1-His12-Hylight647 (middle), or of imaging BCR and MHC class I control microclusters by simultaneously examining Igα-YFP and Cy3-Fab anti–MHC I (bottom). (left) The labeling strategy in the multiple panel two-color TIRF imaging. (right) The growth in FI of microclusters with time, if applicable, is shown schematically. A detailed description for the quantification of FI and the diameter of the microclusters by 2D Gaussian fitting is given in Materials and methods. DIC, differential interference contrast.

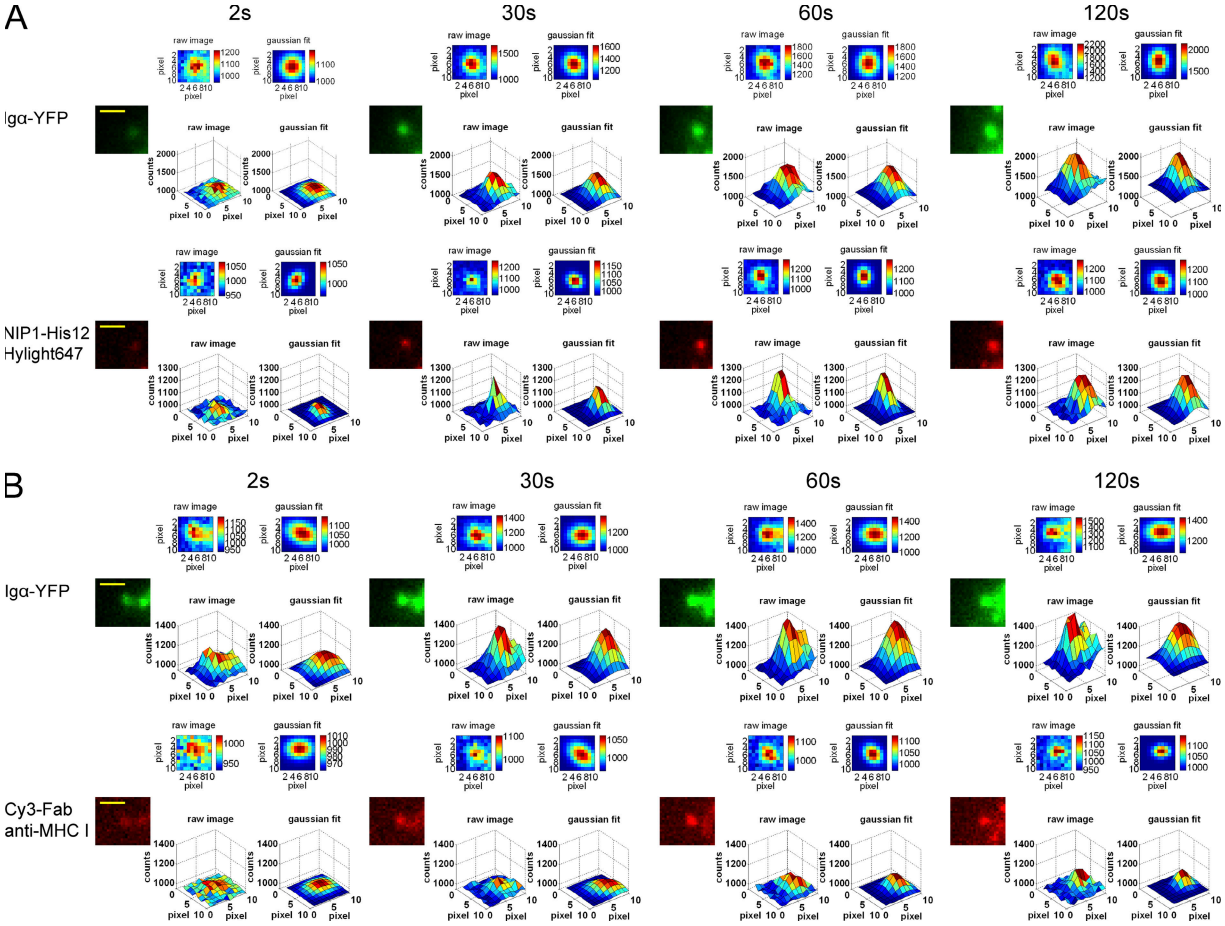

Figure S3. BCR oligomerization–induced growth of BCR microclusters is a selective membrane molecular event. (A) 2.5D Gaussian images of BCR microclusters examined by Igα-YFP (top) or of antigen microclusters examined by NIP1-His12-Hylight647 (bottom) in μ-High J558L cells placed on planar lipid bilayers containing NIP1-His12-Hylight647. (B) 2.5D Gaussian images of BCR microclusters examined by Igα-YFP (top) or by a control surface molecule of Cy3–Fab anti–MHC I (bottom) in μ-High J558L cells placed on planar lipid bilayers containing NIP1-His12. All 2.5D Gaussian images are shown in pseudocolor based on 2D Gaussian fitting of individual microclusters at the indicated time points. For each 2.5D Gaussian image, raw (left) and Gaussian-fitted images (right) are given. Bars, 1.5 μm. Results are representative of three independent experiments.

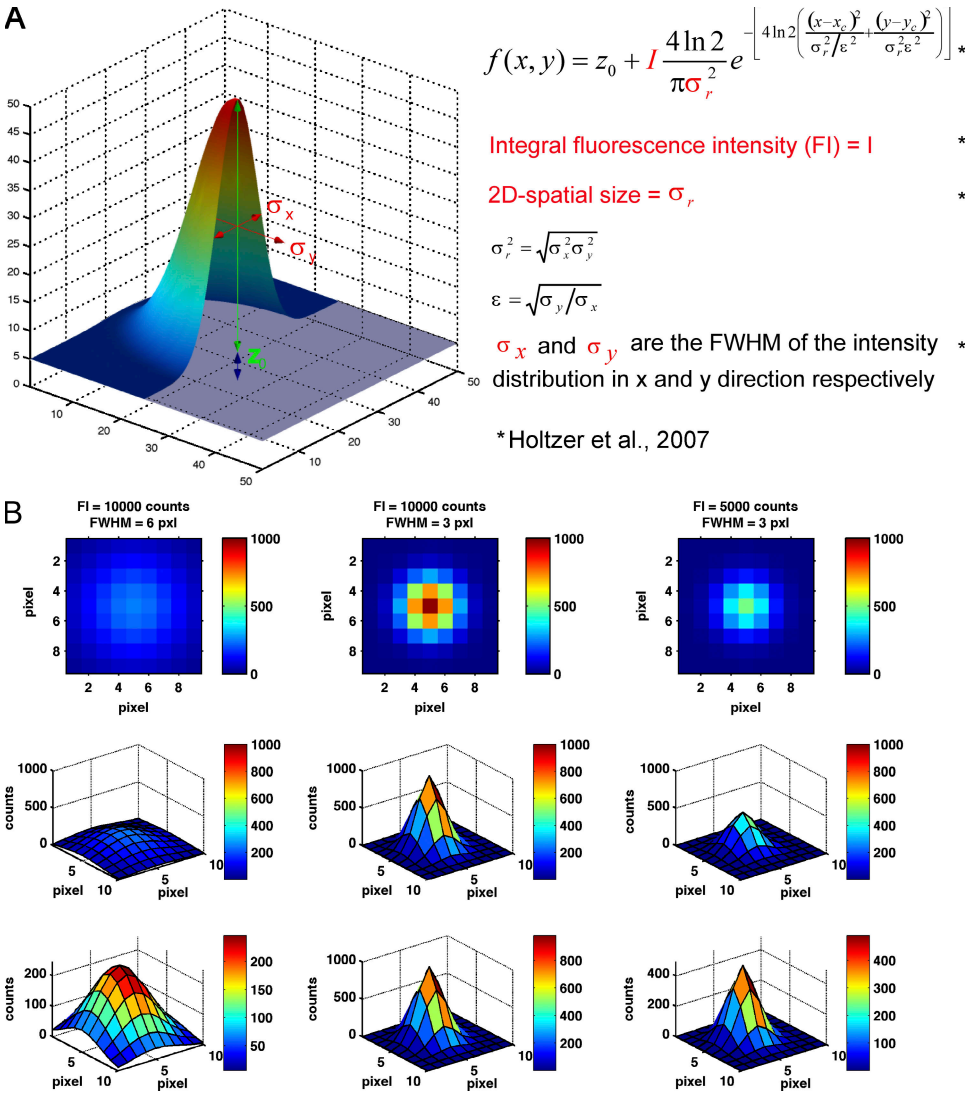

Figure S4. Schematic representation of the 2D Gaussian spreading function and three Gaussian functions in different perspectives. (A) Schematic presentation of the 2D Gaussian spreading function used in this study for the fitting of microclusters, as detailed in Materials and methods (Holtzer et al., 2007). Parameters of FWHM and integrated FI used to quantify the size in terms of diameter and FI of the microclusters are given as indicated. Z_0 values acquired in the function represent the background FIs given for the microclusters in Fig. 3 (B and E) and Fig. 5 (B and E). (B) Three Gaussian functions in different perspectives are shown to illustrate their visual appearance with respect to variations in integrated FI and FWHM. (top) 2D plots (images). The pixel-based intensity values have a range of 0–1,000 counts and are color coded as shown in the color bars. (middle) Pseudo-2.5D Gaussian plots of the first row. (bottom) The same information as the second row, but each plot is scaled by its respective minimum and maximum intensity values. The Gaussian function in the middle column has an FWHM of 3 pixels and an FI of 10,000 counts, which yields a maximum pixel-based intensity value of 982 counts. The Gaussian to the left has the same intensity as but twice the FWHM of the Gaussian in the middle (max. int. = 246 counts), whereas the Gaussian to the right has the same FWHM as but half the intensity of the Gaussian in the middle (max. int. = 491).

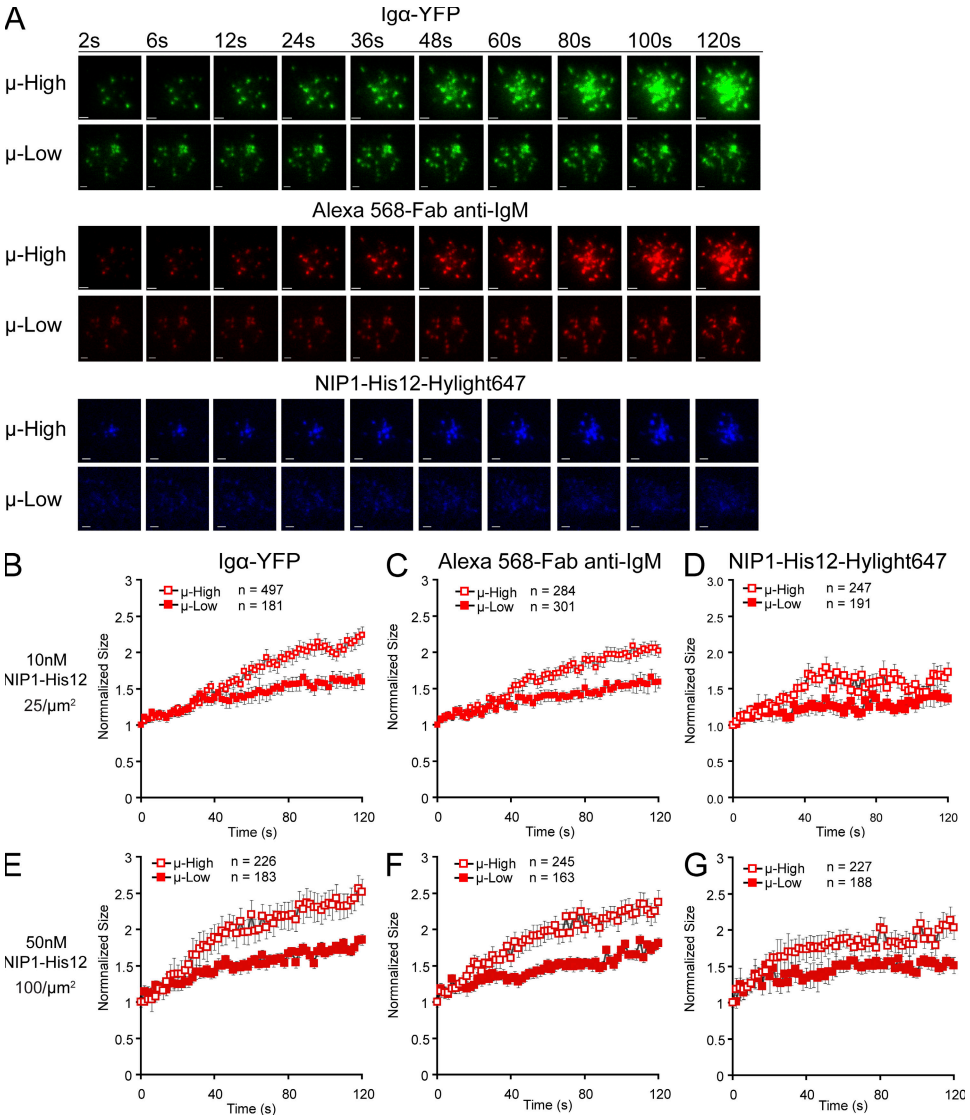

Figure S5. The growth of BCR microclusters is antigen affinity dependent. (A) The growth of BCR microclusters is antigen affinity dependent and results in the enhanced accumulation of BCRs and antigens into the contact area of μ-High J558L cells with antigen-containing lipid bilayers compared with μ-Low J558L cells. Shown are time-lapse TIRF images of μ-High or μ-Low J558L cells examined by Igα-YFP (green) and Alexa Fluor 568–Fab anti-IgM (red) for BCR microclusters, and NIP1-His12-Hylight647 (blue) for antigen microclusters placed on lipid bilayers containing 25 molecules/μm² of NIP1-His12 antigen (Video 8). Bars, 1.5 μm. (B–G) The growth in size of BCR microclusters is antigen affinity dependent. The kinetics of normalized size in 120 s of all of the tracked BCR microclusters examined by Igα-YFP (B and E) and Alexa Fluor 568–Fab anti-IgM (C and F), or the size of antigen microclusters examined by NIP1-His12-Hylight647 (D and G) were shown from μ-High or μ-Low J558L cells placed on planar lipid bilayers containing NIP1-His12 (B, C, E, and F) or NIP1-His12-Hylight647 (D and G) at a concentration of 10 nM (25 molecules/μm²) or 50 nM (100 molecules/μm²), as indicated. In B–G, the data represent means ± SEM of the indicated numbers of microclusters in three independent experiments.

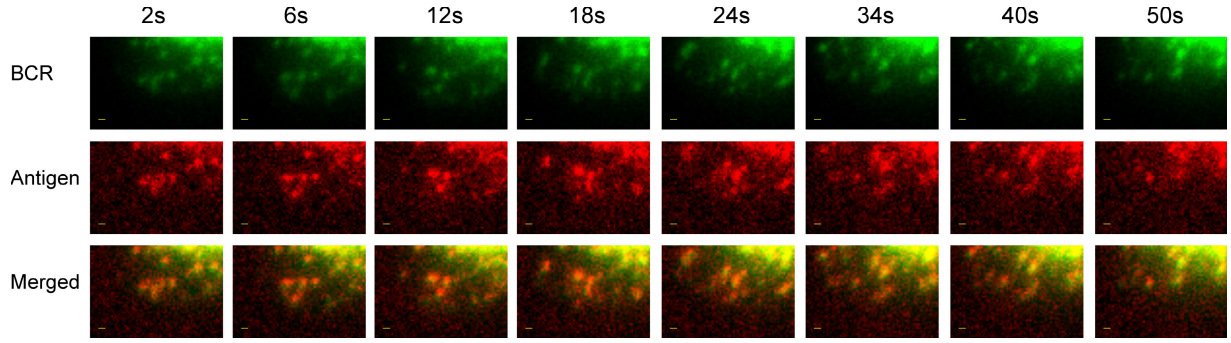

Figure S6. BCR oligomerization induces accumulation of BCR and antigen into BCR microclusters. Shown are time-lapse TIRF images of B1-8 primary B cells examined simultaneously by Alexa Fluor 488–Fab anti-IgM (BCR) for BCR microclusters and NIP1-His12-Hylight647 (antigen) for antigen microclusters placed on NIP1-His12-Hylight647 containing lipid bilayers (Video 9). (bottom) Merged TIRF images of BCR and antigen microclusters. Results are representative of three independent experiments. Bars, 1.5 µm.

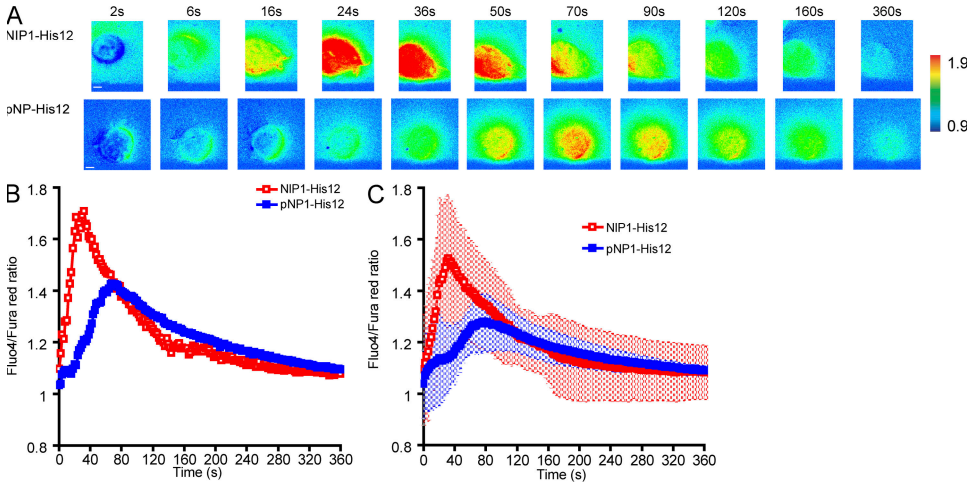

Figure S7. B1-8 primary B cells activated by membrane-bound high affinity antigen NIP1-His12 show faster and stronger calcium influx response compared with low affinity antigen pNP1-His12. (A–C) The calcium responses of B1-8 primary B cells placed on lipid bilayers containing high affinity antigen NIP1-His12 (n = 8) or low affinity antigen pNP1-His12 (n = 8) were measured by time-lapse epifluorescence microscopy. Primary B cells were prelabeled with 2 µg/ml Fluor-4AM and 5 µg/ml FuraRed-AM in the presence of 4 mM probenecid. Calcium levels were expressed as a ratio of Fluo4 to FuraRed FI. Pseudocolor TIRF images showing the typical calcium influx of B1-8 primary B cells are given at the indicated time points (Video 10). Bars, 1.5 µm. Kinetics of the calcium response in 360 s are shown for the presented cells in pseudocolored TIRF images in B (top) or are shown as means ± SD (C) for all of the imaged cells (n = 8 in each condition) in three independent experiments.

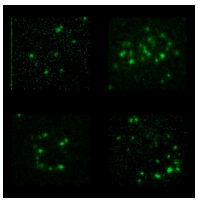

Video 1. High affinity BCRs show an enhanced ability to form immobile oligomers. Single BCR molecule TIRF video showing the mobility of an individual BCR molecule from µ-High (B1-8-High; top) or µ-Low (B1-8-Low; bottom) J558L cells expressing B1-8-BCRs showing 50-fold different affinity for antigen NIP1-His12 ($K_A = 5.2 \times 10^8$ vs. 9.9×10^6) placed on lipid bilayers containing no antigen (left) or NIP1-His12 (right). The video is shown at 28 frames per second (FPS).

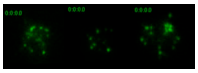

Video 2. Accumulation of BCRs into the contact area between B cells and antigen-containing planar lipid bilayers is affinity dependent, as observed by imaging Igα-YFP. Time-lapse TIRF video showing the real-time responses in 120 s (60 frames with 2-s intervals when imaging) of μ-High (middle) or μ-High (right) J558L cells placed on lipid bilayers containing NIP1-His12 at a concentration of 25 molecules/μm^2. Also shown are the responses of μ-High J558L cells placed on lipid bilayers containing no antigen as a control (left). The acquisitions of BCR–antigen into the contact area with lipid bilayers of both types of cells were examined by imaging Igα-YFP, as detailed in Materials and methods. The video is shown at 10 FPS.

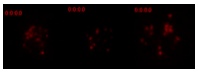

Video 3. Accumulation of BCRs into the contact area between B cells and antigen-containing planar lipid bilayers is affinity dependent, as observed by imaging Alexa Fluor 586–Fab anti-IgM. Time-lapse TIRF video showing the real-time responses in 120 s (60 frames with 2-s intervals when imaging) of μ-High (middle) or μ-Low (right) J558L cells placed on lipid bilayers containing NIP1-His12 at a concentration of 25 molecules/μm^2. Also shown are the responses of μ-High J558L cells placed on lipid bilayers containing no antigen as a control (left). The acquisitions of BCR–antigen into the contact area with lipid bilayers of both types of cells were examined by imaging Alexa Fluor 568–Fab anti-IgM, as detailed in Materials and methods. The video is shown at 10 FPS.

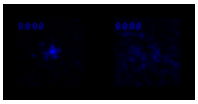

Video 4. Accumulation of antigens into the contact area between B cells and antigen-containing planar lipid bilayers is affinity dependent, as observed by imaging NIP1-His12-Hylight647. Time-lapse TIRF video showing the real-time responses in 120 s (60 frames with 2-s intervals when imaging) of μ-High (left) or μ-Low (right) J558L cells placed on lipid bilayers containing NIP1-His12-Hylight647 at a concentration of 25 molecules/μm^2. The acquisitions of BCR–antigen into the contact area with lipid bilayers of both types of cells were examined by imaging antigen NIP1-His12-Hylight647, as detailed in Materials and methods. The video is shown at 10 FPS.

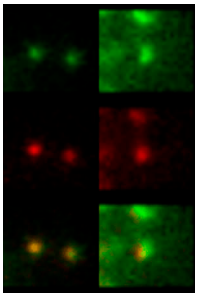

Video 5. BCR microclusters grow with time when encountering antigen-containing lipid bilayers. Time-lapse TIRF video showing the real-time behavior of the typical BCR microclusters from μ-High J558L cells placed on lipid bilayers containing no antigen as control (right) or NIP1-His12 (left) at a concentration of 25 molecules/μm^2. The behaviors of the typical BCR microclusters were examined by simultaneously imaging Igα-YFP (Igα-YFP, green; top) and Alexa Fluor 568–Fab anti-IgM (IgM-Alexa Fluor 568, red; middle). Also shown are the merged images of Igα-YFP and Alexa Fluor 568–Fab anti-IgM (Merged, yellow; bottom). The flashed rectangular region at the beginning of the video indicates the subregion containing the typical BCR microcluster to be amplified for better resolution after the entire video. The imaging time is 120 s (60 frames with 2-s intervals when imaging), and the video is shown at 10 FPS.

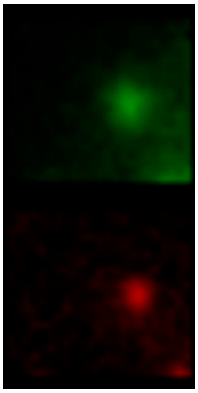

Video 6. Antigen microclusters grow with time when encountering antigen-containing lipid bilayers. Time-lapse TIRF video showing the real-time behavior of the coexamined typical BCR microclusters (BCR, green; top) and antigen microclusters (Antigen, red; bottom) from μ-High J558L cells placed on lipid bilayers containing NIP1-His12-Hylight647 at a concentration of 25 molecules/μm^2. The behavior of the typical BCR and antigen microclusters were examined by simultaneously imaging Igα-YFP (top) and NIP1-His12-Hylight647 (bottom). The flashed rectangular region at the beginning of the video indicates the subregion containing the typical BCR and antigen microclusters to be amplified for better resolution after the entire video. The imaging time is 120 s (60 frames with 2-s intervals when imaging), and the video is shown at 10 FPS.

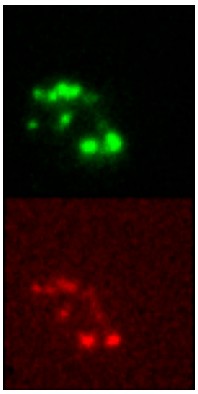

Video 7. The growth of BCR microclusters is selective and excludes MHC class I molecules. Time-lapse TIRF video showing the real-time behavior of the cell and the coexamined typical BCR microclusters (BCR, green; top) and MHC class I microclusters (MHC I, red; bottom) from μ-High J558L cells placed on lipid bilayers containing NIP1-His12 at a concentration of 25 molecules/μm^2. The behavior of acquisition of BCRs only instead of MHC class I control receptor into the contact area of the μ-High J558L cells with the NIP1-His12–containing lipid bilayer were examined by simultaneously imaging Igα-YFP (top) and Cy3–Fab anti–MHC I (bottom). The behavior of the typical BCR and MHC class I microclusters were examined by simultaneously imaging Igα-YFP (top) and Cy3–Fab anti–MHC I (bottom). The flashed rectangular region during the video indicates the subregion containing the typical BCR and antigen microclusters to be amplified for better resolution after the entire video. The imaging time is 120 s (60 frames with 2-s intervals when imaging), and the video is shown at 10 FPS.

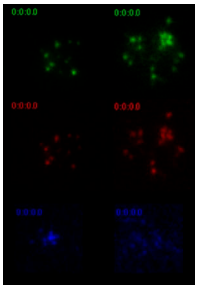

Video 8. The growth of BCR microclusters is antigen affinity dependent. Time-lapse TIRF video showing the real-time behavior of the BCR and antigen microclusters from μ-High (left) or μ-Low (right) J558L cells placed on lipid bilayers containing NIP1-His12 (top and middle) or NIP1-His12-Hylight647 (bottom) at a concentration of 25 molecules/μm^2. The behavior of the BCR and antigen microclusters were examined by simultaneously imaging Igα-YFP (Igα-YFP, green; top) with either Alexa Fluor 568–Fab anti-IgM (IgM-Alexa Fluor 568, red; middle) or NIP1-His12-Hylight647 (Antigen, blue; bottom) in time-lapse TIRF imaging. The imaging time is 120 s (60 frames with 2-s intervals when imaging), and the video is shown at 10 FPS.

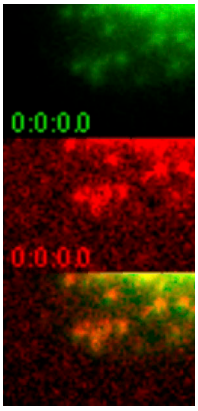

Video 9. The BCR and antigen microclusters in primary B cells grow as they move into the B cell synapse. Time-lapse TIRF video showing the real-time spreading and contraction response and the directed mobility to the center B cell synapse of the coexamined BCR microclusters (BCR, green; top) and antigen microclusters (Antigen, red; middle) from B1-8 primary B cells placed on lipid bilayers containing NIP1-His12-Hylight647 at a concentration of 25 molecules/μm^2. The behaviors of the BCR and antigen microclusters were examined by simultaneously imaging Alexa Fluor 488–Fab anti-IgM (top) and NIP1-His12-Hylight647 (middle). Also shown is the merged image of BCR and antigen microclusters (Merged, yellow; bottom). The imaging time is 50 s (25 frames with 2-s intervals when imaging), and the video is shown at 10 FPS.

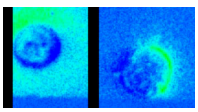

Video 10. B1–8 primary B cells activated by the membrane-bound high affinity antigen NIP1–His12 show faster and stronger calcium responses as compared with B cells activated by the low affinity antigen pNP1–His12. Time-lapse pseudocolored TIRF video showing the calcium influx response of B1-8 primary B cells placed on lipid bilayers containing high affinity antigen NIP1-His12 (left) or low affinity antigen pNP1-His12 (right) at a concentration of 25 molecules/μm^2. B1-8 primary B cells were prelabeled with 2 μg/ml Fluor-4AM and 5 μg/ml FuraRed-AM in the presence of 4 mM probenecid. Calcium levels were expressed as a ratio of Fluo4 to FuraRed Fl. The imaging time is 240 s (60 frames with 2-s intervals when imaging), and the video is shown at 10 FPS.

REFERENCE

Holtzer, L., T. Meckel, and T. Schmidt. 2007. Nanometric three-dimensional tracking of individual quantum dots in cells. *Appl. Phys. Lett.* 90:053902. doi:10.1063/1.2437066